the plant journal

SEB SOCIETY FOR EXPERIMENTAL BIOLOGY

*The Plant Journal* (2024) doi: 10.1111/tpj.17117

# A plastidial lipoyl synthase LIP1p plays a crucial role in phosphate homeostasis in Arabidopsis

**Shenghong Ge[1,†], Xinlong Xiao[2,†], Ke Zhang[2,3], Changhong Yang[2,3], Jinsong Dong[1], Keying Chen[2,3], Qiuyu Lv[1], Viswanathan Satheesh[4] and Mingguang Lei[1,*]**

[1]*College of Life and Environmental Sciences, Hangzhou Normal University, Hangzhou 311121,, China,*

[2]*Shanghai Center for Plant Stress Biology, CAS Center for Excellence in Molecular Plant Sciences, Chinese Academy of Sciences, Shanghai 201602,, China,*

[3]*University of the Chinese Academy of Sciences, Beijing 100049,, China, and*

[4]*Genome Informatics Facility, Office of Biotechnology, Iowa State University, Ames, Iowa 50011, USA*

Received 10 July 2024; revised 8 October 2024; accepted 14 October 2024.

*For correspondence *(e-mail mglei@hznu.edu.cn).

†These authors contributed equally to this work.

## SUMMARY

**Phosphate (Pi) homeostasis is important for plant growth and adaptation to the dynamic environment, which requires the precise regulation of phosphate transporter (PHT) trafficking from the endoplasmic reticulum to the plasma membrane. LIPOYL SYNTHASE 1p (LIP1p) is known as a key enzyme in plastids to catalyze lipoylation of pyruvate dehydrogenase complex for de novo fatty acid synthesis. It is unknown whether this process is involved in regulating Pi homeostasis. Here, we demonstrate a new role of LIP1p in controlling Pi homeostasis by regulating PHT1 trafficking. We recovered a weak mutant allele of *LIP1p* in *Arabidopsis* that accumulates much less Pi and has enhanced expression of phosphate starvation-induced genes. *LIP1p* mutation alters the lipid profile and compromises vesicle trafficking of PHT1 to the plasma membrane to impair Pi uptake. Beside phosphorus, the homeostasis of a series of mineral nutrients was also perturbed in *lip1p* mutant. Our findings provide powerful genetic evidence to support the linkage between lipoylation and ion homeostasis in plants.**

**Keywords: plastidial lipoyl synthase, lipid homeostasis, transporter trafficking, Pi transport, ion homeostasis, *Arabidopsis thaliana*.**

## INTRODUCTION

Phosphorus (P) is one of the essential macronutrients for plant growth and development. However, the available phosphate (Pi) for plants is often scarce in the soil, as most of the P exists as insoluble phosphates or organic forms that cannot be taken up by roots directly (Bieleski, 1973). As sessile organisms, plants have evolved elaborate mechanisms for regulating Pi uptake and usage to cope with the heterogeneous and changing environment. When Pi is deficient, the growth of lateral roots and root hairs is promoted to increase the absorptive surface area (Lopez-Bucio, Cruz-Ramirez, & Herrera-Estrella, 2003; Peret et al., 2014). More acid phosphatase and organic acids are induced and secreted to release Pi from the immobilized P in the soil (Tran, Hurley, & Plaxton, 2010; Wang et al., 2011). Anthocyanin accumulates on the plant leaves to protect them from photodamage (Burger & Edwards, 1996; Lei et al., 2011; Vance, Uhde-Stone, & Allan, 2003).

Under Pi starvation, the high-affinity Pi transporters (PHTs) are induced to increase Pi influx. There are nine PHT1 (PHT1; 1–9) members with partial function redundancy in Arabidopsis, with PHT1;1 and PHT1;4 as the major transporter proteins for uptake of rhizosphere Pi under Pi-sufficient and Pi-deficient conditions (Misson, Thibaud, Bechtold, Raghothama, & Nussaume, 2004; Shin, Shin, Dewbre, & Harrison, 2004). The PHT1s are regulated not only at transcriptional but posttranslational levels. Eight of the nine PHT1 coding genes have at least one *cis*-element P1BS (PHR1-binding site) in their promoter. PHR1, the central regulator, could bind to P1BS and activate PHT1 gene expression. After translation in the endoplasmic reticulum (ER), the PHT1 proteins are trafficked to the plasma membrane (PM) with the help of PHF1 (phosphate transporter traffic facilitator 1), which is also induced by Pi starvation. In the absence of PHF1, PHT1s are retained in ER, and Pi uptake is seriously compromised (Bayle et al., 2011;

González, Solano, Rubio, Leyva, & Paz-Ares, 2005). Under Pi-sufficient conditions, phosphorylation of PHT1s by casein kinase II at the C-terminal inhibits their interaction with PHF1, thereby impairing their trafficking from the ER to the PM (Bayle et al., 2011; Chen et al., 2015). Furthermore, PHT1 proteins can be internalized from the PM into endosomes and directed for degradation in the vacuole with the ESCRT-III-Associated Protein ALIX (Bayle et al., 2011; Cardona-López et al., 2015). In contrast, under Pi-limiting conditions, dephosphorylation of PHT1 by the phosphatase PP95 promotes PHT1 trafficking from ER to PM when Pi is deficient (Yang et al., 2020).

The trafficking of membrane proteins from the ER to the PM is carried out by the vesicles, which are compartments formed by a lipid bilayer. It has been reported that phosphatidylinositol (PI), sphingolipids and phosphatidic acids (PAs), and phosphatidylcholines (PCs) play important roles in vesicle trafficking, including vesicle budding, transport, exocytosis, endocytosis, and fusion (Gao et al., 2017; Li & Xue, 2007; Melser et al., 2011). In this study, we performed a forward genetic screen in *Arabidopsis* to identify new factors involved in Pi homeostasis. We identified LIP1p, the lipoyl synthase in plastid, as a novel regulator of PHT1 trafficking. The expression of *PHT1;4* and other Pi starvation-induced (PSI) genes was constitutively upregulated in the *lip1p* mutant. The deficiency of LIP1p resulted in reduced trafficking of PHT1 to the PM and a corresponding decrease in Pi content in the *lip1p* mutant.

## RESULTS

### Isolation of the *phod2* mutant

We previously reported an efficient reporter-based genetic screen for cellular factors involved in Pi homeostasis. In this system, a firefly luciferase (*LUC*) reporter gene was driven by the *PHT1;4* promoter (*pPHT1;4::LUC*) and transformed into Arabidopsis Col-0 (Figure S1). Under Pi starvation, the *LUC* reporter was induced in the transgenic line (thereafter referred as WT) and a fluorescence signal was recorded (Figure S1) (Karthikeyan *et al.*, 2002; Lei et al., 2011). The WT seeds were mutagenized by ethyl methanesulfonate (EMS) and $M_2$ seedlings were screened on HP (high phosphate) and LP (low phosphate) media for mutants with altered LUC signal (Figure S1). This screening led to the isolation of *phosphate deficiency1* (*phod1*) (Xiao et al., 2022). In this study, we report the characterization of the *phod2* mutant. In the *phod2* mutant, *pPHT1;4::LUC* expression was elevated compared to WT under both HP and LP conditions (Figure 1a). We then analyzed the transcript levels of the endogenous *PHT1;4* gene by RT-qPCR, which revealed significant upregulation of *PHT1;4* expressions under both conditions (Figure 1b). These results suggest that the gene mutated in *phod2* plays an important role in regulating *PHT1;4* gene expression.

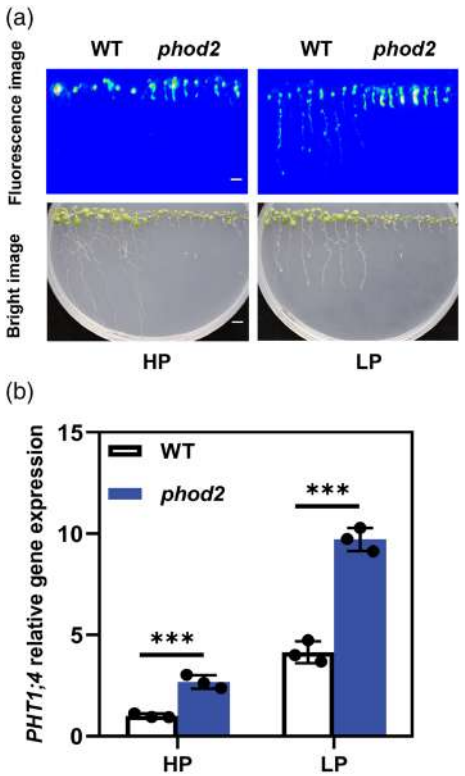


**Figure 1.** Analysis of *PHT1;4* expression in WT and *phod2* seedlings.
(a) The expression of the reporter gene (*pPHT1;4::LUC*) in 10-day-old WT and *phod2* seedlings on HP (625 μM) or LP (150 μM) media which was indicated by luminescence signals. Scale bars: 0.5 cm.
(b) Relative expression of endogenous *PHT1;4* gene in WT and *phod2* seedlings on HP or LP media. The data are means ± SD. $n = 3$ (biological replicates). ***$P < 0.001$. Two-tailed *t*-test.

### The *phod2* mutation enhances PSI gene expression

In addition to *PHT1;4*, we examined the expression of five other PSI genes in seedlings grown on HP or LP media and found that the transcript levels of all these genes were dramatically increased in *phod2* mutant compared to WT under both HP and LP conditions (Figure 2a). Further transcriptome analysis revealed that the *phod2* mutation led to the increased expression of 420 and 478 genes under HP and LP conditions, respectively. Among these upregulated genes, 194 (46%) under HP and 190 (40%) under LP conditions were identified as Pi starvation-induced (PSI) genes (Figure 2b,c; Data Set1). GO analysis of these upregulated genes in *phod2* mutant showed that it was significant for these genes associated with phosphate homeostasis as well as transport of other ions or lipids (Figure 2d). These results indicate that PHOD2 widely regulated the expression of PSI genes.

### Pi homeostasis is perturbed in the *phod2* mutant

In addition to the misregulation of PSI genes, the *phod2* mutant also exhibited other constitutive Pi starvation

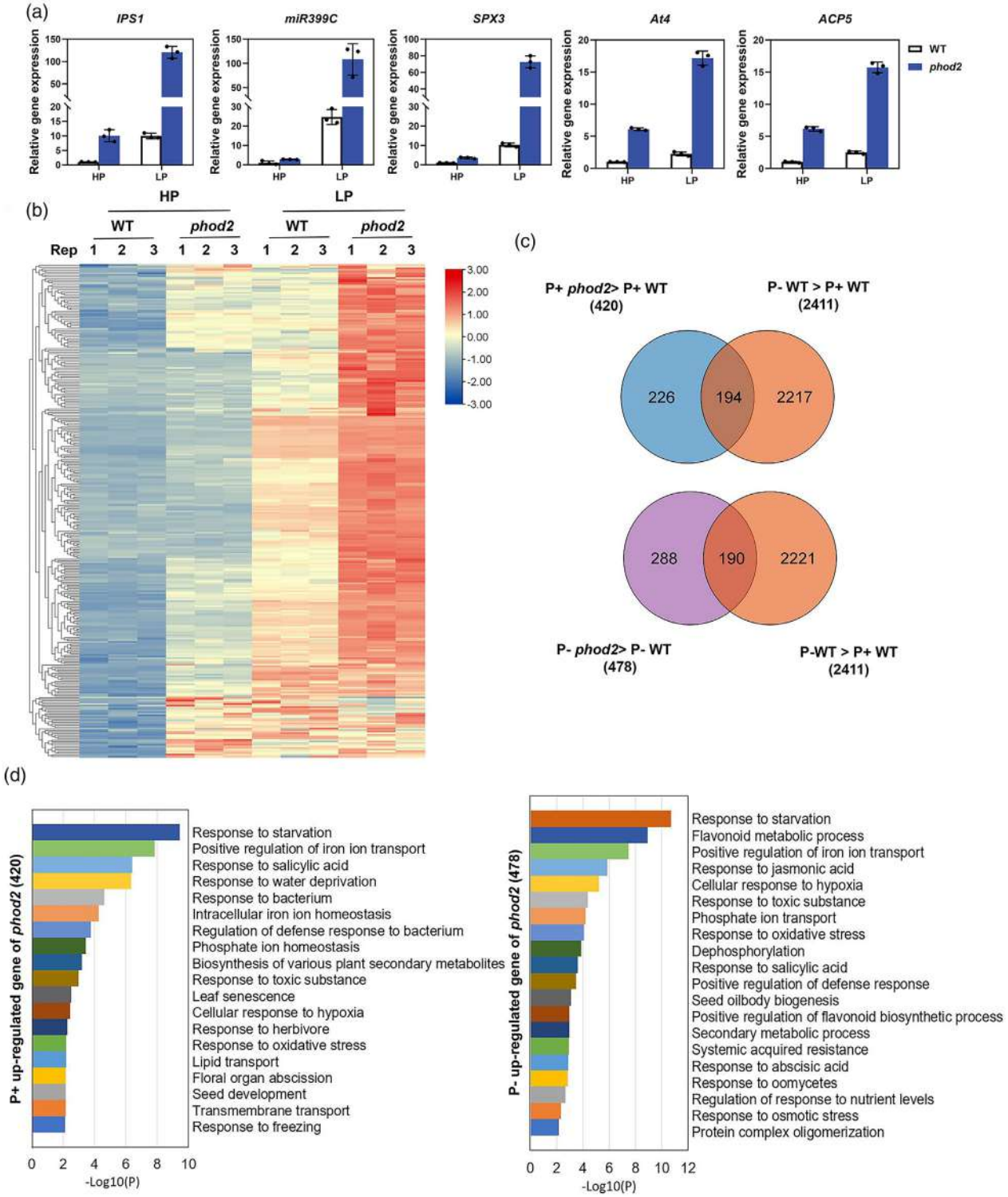


**Figure 2.** A large number of PSI genes are induced in *phod2* mutant.
(a) Quantitative PCR analysis of classical PSI genes expression in WT and *phod2* on an HP or LP medium. The data are means ± SD. Three biological replicates. The foldchanges of transcript levels are normalized to WT (HP).
(b) Heatmap cluster of transcripts of PSI genes which upregulated in the *phod2* mutant grown on HP and LP media.
(c) Venn diagram showing the overlap number of genes upregulated by Pi deficiency and *phod2* mutagenesis.
(d) GO analysis of upregulated genes in *phod2* mutant.

response (PSR) phenotypes under HP and LP conditions. Anthocyanin accumulation is a typical plant response to Pi starvation. When grown on an LP medium for 8 days, the leaves of WT turned light purple, whereas that of the *phod2* mutant became dark purple. Even under HP conditions, the *phod2* mutant accumulated visible levels of anthocyanin in leaves (Figure 3a). *F3H*, *LDOX*, and *UF3GT* are key genes for anthocyanin synthesis under LP conditions. They were all highly induced in *phod2* under both LP and HP conditions (Figure 3b). Consistent with the phenotype, quantitative analysis showed that the anthocyanin content was much higher in the shoot of *phod2* than in WT under both conditions (Figure 3c). The *phod2* mutant also exhibits abnormal growth and development, including shortened primary roots (Figure S2a), dwarfing of plants (Figure S2b,d), lower biomass (Figure S2e), and defects in embryonic development resulting in low fertility (Figure S2c). The *phod2* mutation also increased both the length and density of root hair (Figure S2f). Furthermore, we found that the Pi content was dramatically decreased in *phod2* mutant both in the shoot and root compared to that in WT (Figure 3d; Figure S2g). These results suggested that *phod2* mutation perturbed Pi homeostasis and activated PSI gene expression.

### *phod2* is a weak allele of *LIP1p*

To find out the causative mutation for the increased *pPHT1;4::LUC* expression, the *phod2* mutant was backcrossed to WT, and the genomic DNA from the pooled $F_2$ seedlings with increased LUC signal was subjected to high-throughput sequencing. The data were analyzed following a mapping-by-sequencing workflow and a point mutation was identified in *LIPOYL SYNTHASE 1* (*LIP1p*) gene (AT5G08415) and confirmed using Sanger sequencing (Figure 4a). LIP1p is the plastidial lipoyl synthase and it was reported that the knockout of *LIP1p* is embryo-lethal. Although *phod2* showed some development defects, it could complete the life cycle, suggesting that *phod2* is a weak allele of *LIP1p*. The mutation in *phod2* substitutes A for G at the last nucleotide of the fifth exon without a change of amino acid residue. This substitution may affect the splicing efficiency of the fifth intron (Figure 4b). To confirm this hypothesis, we designed a forward primer on the fifth exon and a reverse one on the seventh exon to amplify the fragment with the cDNAs as the PCR templates. The results showed that a PCR product of about 350 bp was amplified from WT. However, most of the products from *phod2* shifted to ~500 bp, indicating an intron was retained in most *LIP1p* transcripts in *phod2* mutant (Figure 4c,d). The PCR product was sequenced to confirm the retention of the fifth intron, resulting in a premature stop codon (Figure 4b). We used RT-qPCR to examine the levels of different transcripts with specific primers and found that the intron-containing transcript was dominant in *phod2* mutant, consistent with the results of agarose gel electrophoresis (Figure 4c–e). RNA structure prediction with RNAfold in the Vienna package (Ver.2.4.3) shows that base substitution A for G results in a double-stranded RNA structure (pointed by a blue arrow, Figure S3c) while the position in WT *LIP1p* RNA showing a single-stranded structural (pointed by a red arrow) (Figure S3b) (Lorenz et al., 2011). When the two-nucleotides are double-stranded RNA structures, introns are not easy to splicing (Gosai et al., 2015; Liu et al., 2021). RNA structural analysis provides an explanation that the synonymous mutation in *phod2* causes the disruption of *LIP1p* RNA splicing.

To further confirm that the *phod2* phenotypes are due to the loss of function of the *LIP1p* gene, we transformed

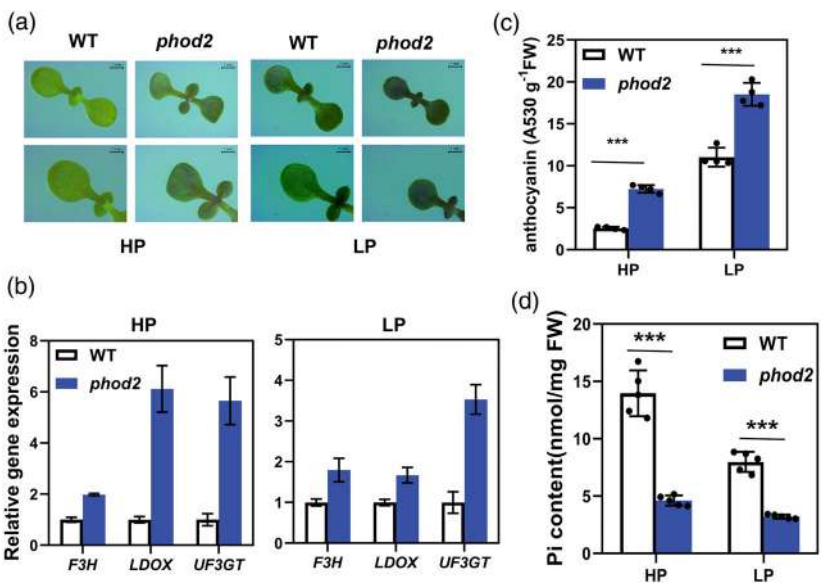


**Figure 3.** Pi homeostasis was destructive in the *phod2* mutant.
(a) Anthocyanin phenotypes of WT and *phod2* on HP or LP conditions. Scale bars: 1 mm. Eight-day-old seedlings.
(b) Quantitative real-time PCR analysis of *F3H*, *LDOX*, and *UF3GT* transcript levels in WT and *phod2* seedlings grown on HP or LP conditions. The data are means ± SD. $n = 3$ (biologically independent replicates).
(c) Anthocyanin contents of WT and *phod2*. FW, fresh weight. The data are means ± SD. $n = 4$. $^{***}P < 0.001$, two-tailed *t*-test.
(d) Pi content of 8-day-old seedlings of the WT and the *phod2* mutant. The data are means ± SD. $n = 5$ (biologically independent replicates). $^{*}P < 0.05$, $^{**}P < 0.01$, $^{***}P < 0.001$, two-tailed *t*-test.

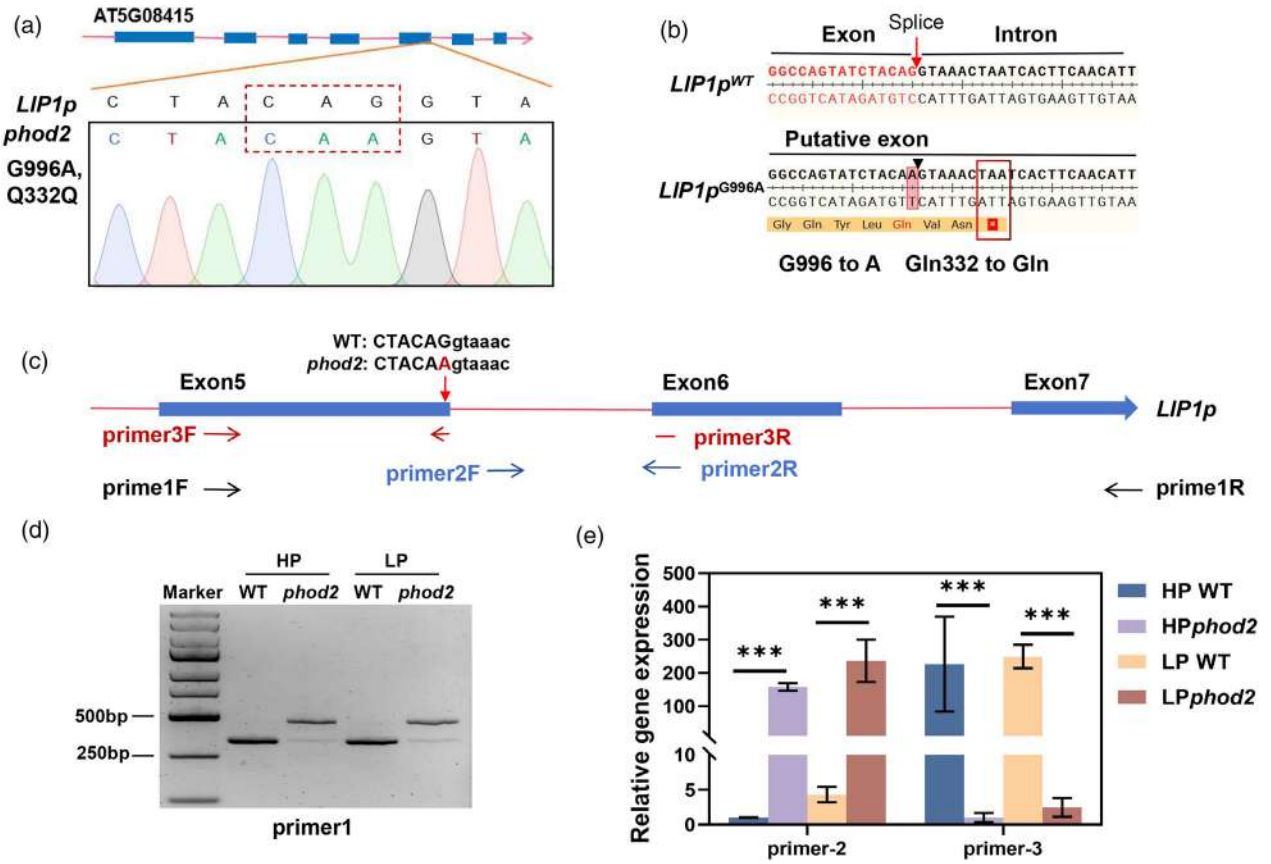


**Figure 4.** Identification of the causal gene mutation in *phod2*.
(a) Schematic diagram and Sanger sequencing chromatogram showing single-base mutation (G996A) in *phod2*.
(b) Sanger sequencing showed that the intron behind the mutation site was still retained in the CDS of *phod2*. The red rectangle shows the stop codon location.
(c) Schematic diagram of the primer target sites. The red arrow points out the position of single-base substitution in *LIP1p*.
(d) The single-base substitution results in two transcripts with different lengths in the *phod2* mutant. The black arrow in (c) represents the position of the Primer1.
(e) Two kinds of transcript levels of endogenous *LIP1p* gene were detected using corresponding location primers. Primer2: 2F is located at the fifth intron, 2R is located at the joint of fifth intron and sixth exon. Primer3: 3F is located at the fifth exon, half of the 3R is located on the fifth exon, and the other half on the sixth exon. ***$P < 0.001$, two-tailed *t*-test.

FLAG-tagged *LIP1p* genomic DNA, driven by its native promoter into the *phod2* mutant. This transformation fully rescued the *phod2*-mutant phenotypes, including the short root (Figure 5a,b), the enhanced expression of PSI genes (Figure 5c), the reduced Pi content in seedlings (Figure 5d), and the overaccumulation of anthocyanin in the shoot (Figure 5e,f).

### LIP1p is important for PHT1 trafficking

Plasma membrane-localized PHT1 transporters in root are responsible for the uptake of Pi, with PHT1;1 and PHT1;4 as the major transporters which account for about 75% capacity in Pi acquisition from environments (Shin et al., 2004). Under Pi starvation, PHT1;1-GFP and PHT1;4-GFP are mainly localized at the plasma membrane. However, the introduction of the *phod2* mutation decreased the GFP signal at the plasma membrane and more PHT1;1-GFP and PHT1;4-GFP was found in the cytoplasm (Figure 6a,b), indicating that *phod2* mutation compromised PHT1 trafficking. Western blot also showed that PHT1;1 and PHT1;4 proteins were significantly decreased in *phod2* compared to that in WT (Figure 6c,d). The trafficking inhibitor Brefeldin A (BFA) induces the *trans*-Golgi network (TGN) and early endosome to incorporate into the BFA compartment. After BFA treatment for 2 h, PHT1;4-GFP aggregated in the BFA compartment. However, PHT1;4-GFP could not be clearly detected in the BFA compartment in *phod2* mutant, indicating that PHT1;4 was retained in ER or *cis*-Golgi cisternae (Figure 6e). To verify that the Pi content reduction in the mutant is due to the decreased levels of PHT1 at the plasma membrane, we attempted to increase its expression in *phod2* by overexpressing *PHT1;1*. In the *35S::PHT1;1-GFP/phod2* transgenic line, PHT1;1-GFP levels were showing increased in both

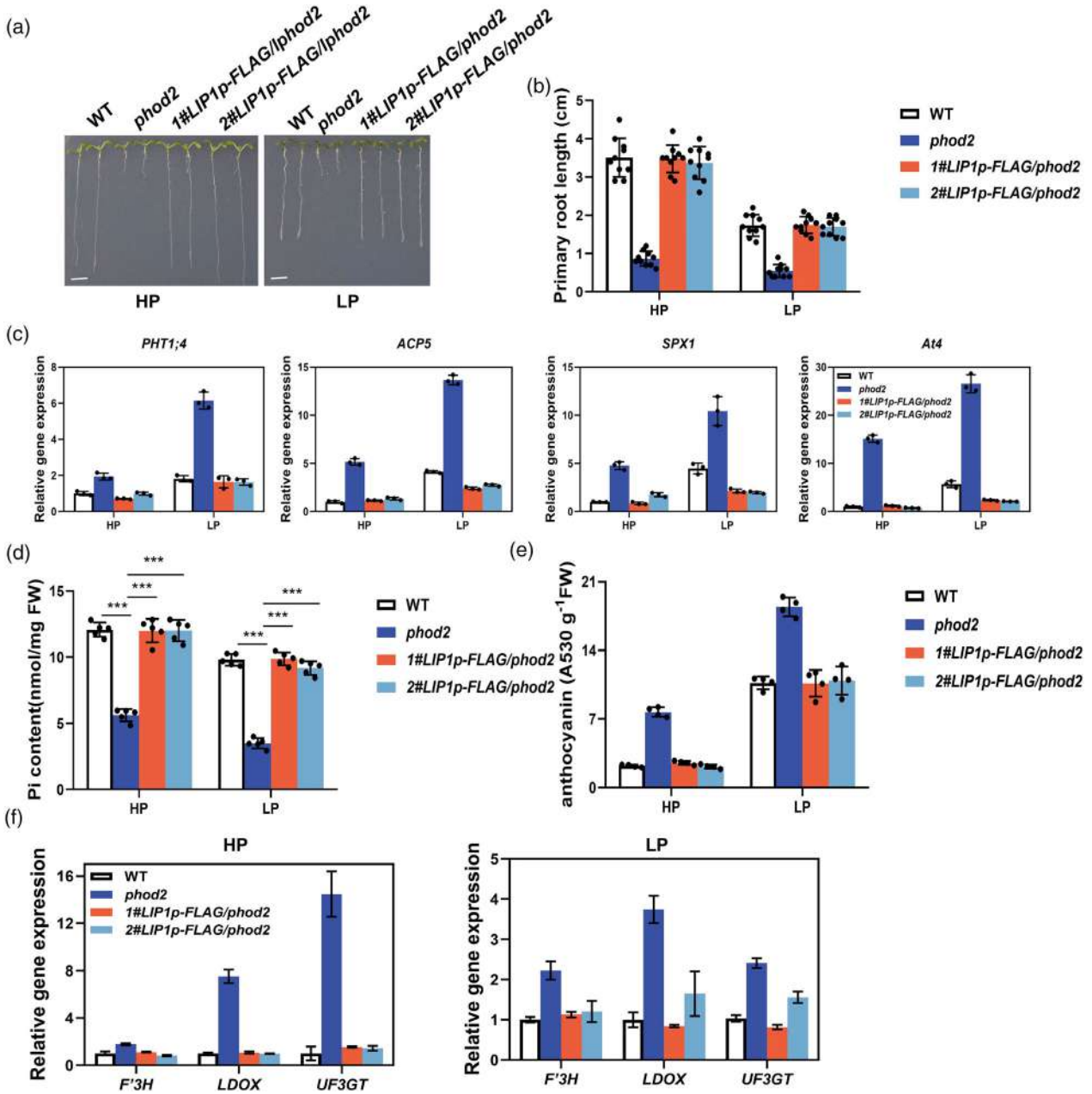


**Figure 5.** LIP1 is required for Pi homeostasis and starvation response.
(a, b) The root phenotype among the WT, the *phod2* mutant, and the *phod2* mutant was transformed with *LIP1p-FLAG* driven by its native promoter on HP or LP conditions. Scale bars: 0.5 cm.
(c) Quantitative PCR analysis of PSI gene expression in 8-day-old seedlings of different genotypes shown in (a) grown on HP or LP medium.
(d) Pi content of different genotypes shown in (a). The data are means ± SD. $n = 5$ (biologically independent replicates). ***$P < 0.001$, two-tailed *t*-test.
(e) Anthocyanin contents of different genotypes are shown in (a). FW, fresh weight.
(f) Quantitative PCR analysis of *F'3H*, *LDOX*, and *UF3GT* transcript levels in different genotypes shown in (a) on HP or LP conditions. The data are means ± SD. $n = 3$ (biologically independent replicates).

cytoplasm and plasma membrane compared to *pPHT1;1::PHT1;1-GFP/phod2* (Figure S4d). The cellular Pi content in the *PHT1;1* overexpression lines were significantly higher than that in *phod2* mutant, but still lower than that in WT (Figure S4a,b). These results indicate LIP1p is an important regulator of PHT1 trafficking to maintain Pi homeostasis.

### Lipidomics of *phod2* mutant

LIP1p is a plastid-specific isoform of lipoyl synthase essential for lipoylation of pyruvate dehydrogenase complex, which generates acetyl-CoA for de novo fatty acid biosynthesis and lipogenesis in plants. Therefore, lipidomic

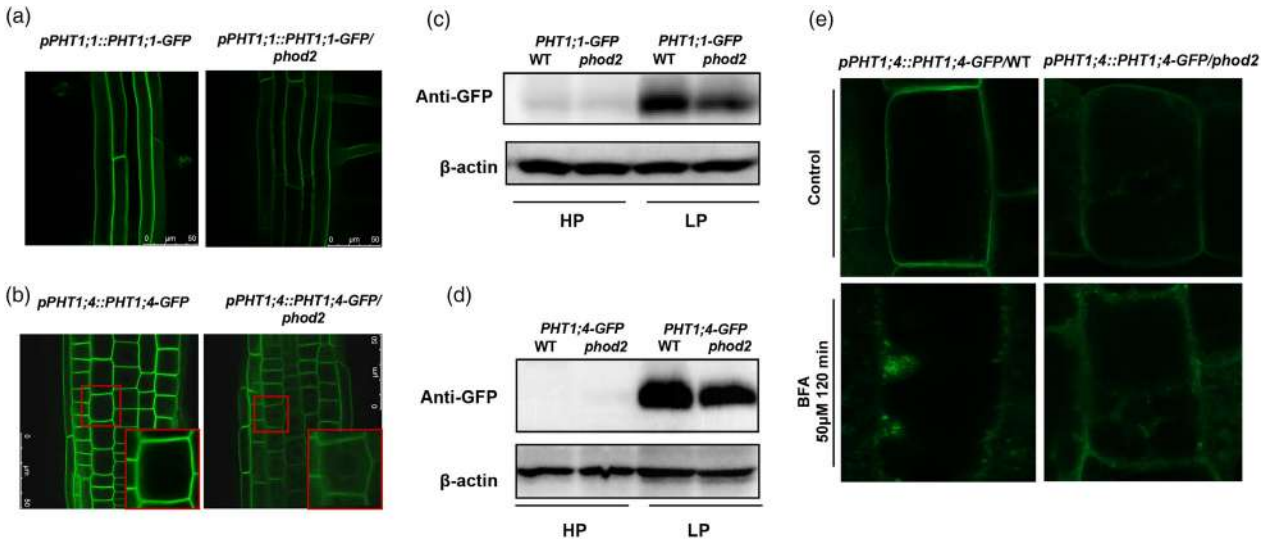


**Figure 6.** Absence of LIP1p impaired the accumulation of phosphate transporters in the plasma membrane of *phod2*.
(a, b) Accumulation of PHT1;1-GFP (a) and PHT1;4-GFP (b) in WT and *phod2*. Scale bars: 50 μm. The red box indicates enlarged images.
(c, d) Western blot analysis of PHT1;1-GFP (c) and PHT1;4-GFP (d) in roots of the WT and *phod2* mutant. β-actin was used as a loading control.
(e) Trafficking blocking of PHT1;4-GFP by BFA treatment in root epidermal cells of WT and *phod2*. The green bright spots represent the BFA bodies in which PHT1;4-GFP are retention during the protein trafficking from the endoplasmic reticulum.

analysis was carried out in the *phod2* mutant and WT. Totally, 914 lipid species were detected in both WT and *phod2* and classified into 50 classes with various numbers, such as 231 triacylglycerols (TG), 172 ceramides (Cer), 61 sulfoquinovosyl diacylglycerols (SQDG), etc. (Data Set S1).

We found 235 lipid species were increased while 247 decreased in *phod2* mutant compared to WT (Figure 7a,b). These differential expression (DE) species were mapped to 40 classes and classified into six lipid categories (Glycerolipids, GL; Glycerophospholipids, GP; Sphingolipids, SP; Saccharolipids, SL; Sterol Lipids, ST; Fatty acids, FA) (Figure 7c). We have detected eight species in the FA category, of which four were significantly increased, while two decreased in *phod2* (Figure S5). By analyzing the top 30 downregulated lipid species in *phod2*, we found that most are glycerophospholipids (GP), including PG (38:7), LPC (18:3), PA (18:3_20:3), PI (29:0), etc. (Figure 7d,e). In contrast, by analyzing the top 30 upregulated lipid species in *phod2*, we found most are Saccharolipids (SL) and Glycerolipids (GL), such as SQDG (46:0), SQMG (34:5) and TG (11:0_11:2_11:3) (Figure 7f,g). Interestingly, phospholipids (PG, PC, PA, PI, PE, etc.) were significantly decreased in the *phod2* mutant, while the sulpholipids SQDG and SQMG were significantly increased (Figure 7b; Figure S5). Overexpressing of PHT1;1 not only increased Pi content (Figure S4b) but also greatly changed the lipidomics of the *phod2* mutant (Figure S6a,b). The Venn diagrams and heat maps show that only 60 of the 247 downregulated and 18 of the 235 upregulated lipid species in *phod2* mutant were rescued by overexpressed PHT1;1 (Figure S6c–f). These data indicate that the change of lipidomics in *phod2* mutant is partially dependent on the reduced Pi content.

### LIP1p regulates ion homeostasis

Phosphatidic acid and sphingolipids have been reported to be involved in the regulation of vesicle trafficking of transporter proteins (Li & Xue, 2007; Melser et al., 2011). In addition to phosphate, the disruption of lipid homeostasis may also jeopardize the uptake of other elements. Therefore, we performed the ionome analysis of *phod2* and WT. Consistent with the results of Pi content, total phosphorus (P) was significantly decreased in *phod2* compared to the WT. Besides P, we found that the content of K, Ca, Mg, Fe, Mo, Sr, and Rb is also significantly decreased in the mutant *phod2* (Figure 8). Consistently, several ion transporters were also induced by *phod2* mutation (Figure S8). These results indicate that LIP1p-regulated lipid metabolism plays an important role in ion homeostasis.

## DISCUSSION

Lipoic acid (LA) is an important cofactor for five multi-enzyme complexes: pyruvate dehydrogenase (PDH), ketoglutarate dehydrogenase (KGDH), branched-chain ketoacid dehydrogenase (BCDH), acetate dehydrogenase (AoDH), and glycine decarboxylase (GDC) (Douce, Bourguignon, Neuburger, & Rebeille, 2001; Mooney, Miernyk, & Randall, 2002; Perham, 2000). In plants, lipoylation mainly happened in mitochondria where octanoyltransferase LIP2 uses de novo-synthesized octanoyl groups bound to acyl

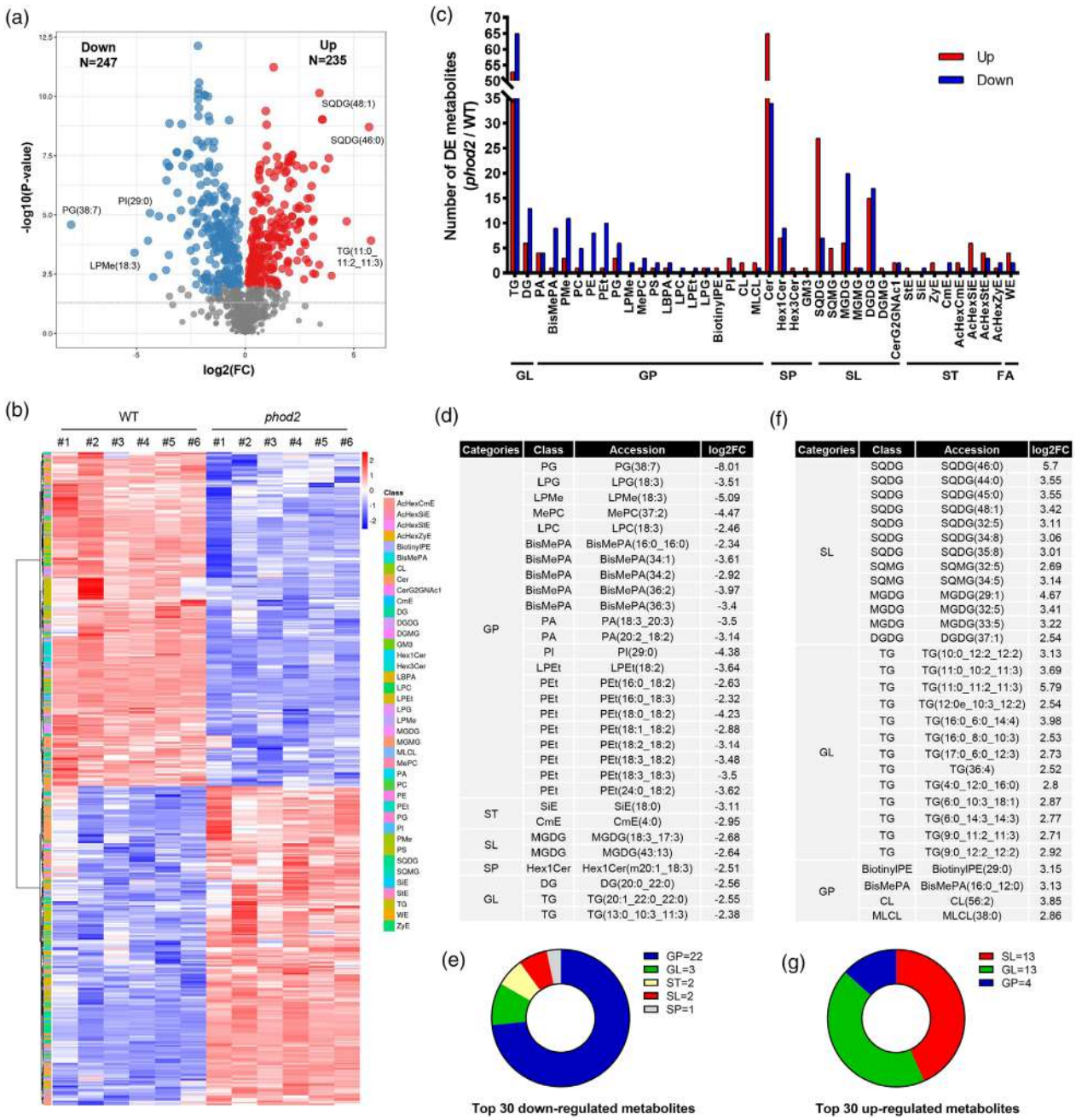


| Categories | Class | Accession | log2FC |
|---|---|---|---|
| GP | PG | PG(38:7) | -8.01 |
| | LPG | LPG(18:3) | -3.51 |
| | LPMe | LPMe(18:3) | -5.09 |
| | MePC | MePC(37:2) | -4.47 |
| | LPC | LPC(18:3) | -2.46 |
| | BisMePA | BisMePA(16:0_16:0) | -2.34 |
| | BisMePA | BisMePA(34:1) | -3.61 |
| | BisMePA | BisMePA(34:2) | -2.92 |
| | BisMePA | BisMePA(36:2) | -3.97 |
| | BisMePA | BisMePA(36:3) | -3.4 |
| | PA | PA(18:3_20:3) | -3.5 |
| | PA | PA(20:2_18:2) | -3.14 |
| | PI | PI(29:0) | -4.38 |
| | LPEt | LPEt(18:2) | -3.64 |
| | PEt | PEt(16:0_18:2) | -2.63 |
| | PEt | PEt(16:0_18:3) | -2.32 |
| | PEt | PEt(18:0_18:2) | -4.23 |
| | PEt | PEt(18:1_18:2) | -2.88 |
| | PEt | PEt(18:2_18:2) | -3.14 |
| | PEt | PEt(18:3_18:2) | -3.48 |
| | PEt | PEt(18:3_18:3) | -3.5 |
| | PEt | PEt(24:0_18:2) | -3.62 |
| ST | SiE | SiE(18:0) | -3.11 |
| | CmE | CmE(4:0) | -2.95 |
| SL | MGDG | MGDG(18:3_17:3) | -2.68 |
| | MGDG | MGDG(43:13) | -2.64 |
| SP | Hex1Cer | Hex1Cer(m20:1_18:3) | -2.51 |
| GL | DG | DG(20:0_22:0) | -2.56 |
| | TG | TG(20:1_22:0_22:0) | -2.55 |
| | TG | TG(13:0_10:3_11:3) | -2.38 |

| Categories | Class | Accession | log2FC |
|---|---|---|---|
| SL | SQDG | SQDG(46:0) | 5.7 |
| | SQDG | SQDG(44:0) | 3.55 |
| | SQDG | SQDG(45:0) | 3.55 |
| | SQDG | SQDG(48:1) | 3.42 |
| | SQDG | SQDG(32:5) | 3.11 |
| | SQDG | SQDG(34:8) | 3.06 |
| | SQDG | SQDG(35:8) | 3.01 |
| | SQMG | SQMG(32:5) | 2.69 |
| | SQMG | SQMG(34:5) | 3.14 |
| | MGDG | MGDG(29:1) | 4.67 |
| | MGDG | MGDG(32:5) | 3.41 |
| | MGDG | MGDG(33:5) | 3.22 |
| | DGDG | DGDG(37:1) | 2.54 |
| GL | TG | TG(10:0_12:2_12:2) | 3.13 |
| | TG | TG(11:0_10:2_11:3) | 3.69 |
| | TG | TG(11:0_11:2_11:3) | 5.79 |
| | TG | TG(12:0e_10:3_12:2) | 2.54 |
| | TG | TG(16:0_6:0_14:4) | 3.98 |
| | TG | TG(16:0_8:0_10:3) | 2.53 |
| | TG | TG(17:0_6:0_12:3) | 2.73 |
| | TG | TG(36:4) | 2.52 |
| | TG | TG(4:0_12:0_16:0) | 2.8 |
| | TG | TG(6:0_10:3_18:1) | 2.87 |
| | TG | TG(6:0_14:3_14:3) | 2.77 |
| | TG | TG(9:0_11:2_11:3) | 2.71 |
| | TG | TG(9:0_12:2_12:2) | 2.92 |
| GP | BiotinylPE | BiotinylPE(29:0) | 3.15 |
| | BisMePA | BisMePA(16:0_12:0) | 3.13 |
| | CL | CL(56:2) | 3.85 |
| | MLCL | MLCL(38:0) | 2.86 |

**Figure 7.** Disorder of lipid metabolic in *phod2*.
(a) The volcano plot shows the differentially expressed lipid metabolites in *phod2* compared with WT. FC, foldchange.
(b) Agglomerate hierarchical clustering heat map indicates the DE metabolites in WT and *phod2*. 14-day-old seedlings grown on an HP medium. The columns represent the samples and the rows represent the lipid metabolites.
(c) Count the number of different expression (DE) metabolites in 40 kinds of lipid classes.
(d) List of top 30 downregulated lipid metabolites.
(e) Categories analysis of top 30 downregulated lipid metabolites.
(f) List of top 30 upregulated lipid metabolites.
(g) Categories analysis of top 30 upregulated lipid metabolites. GL, glycerolipids; GP, glycerophospholipids; SP, Sphingolipids; SL, Saccharolipids; ST, sterol lipids, FA, fatty acyls.

carrier protein (ACP) to trans-octanoylate target proteins and lipoyl synthase LIP1 subsequently inserts two sulfur atoms of S-adenosylmethionine into the C-6 and C-8 positions of the target protein-bound octanoyl group (Wada, Yasuno, Jordan, Cronan, & Wada, 2001; Yasuno & Wada, 1998). However, PDH also functions in plastids to

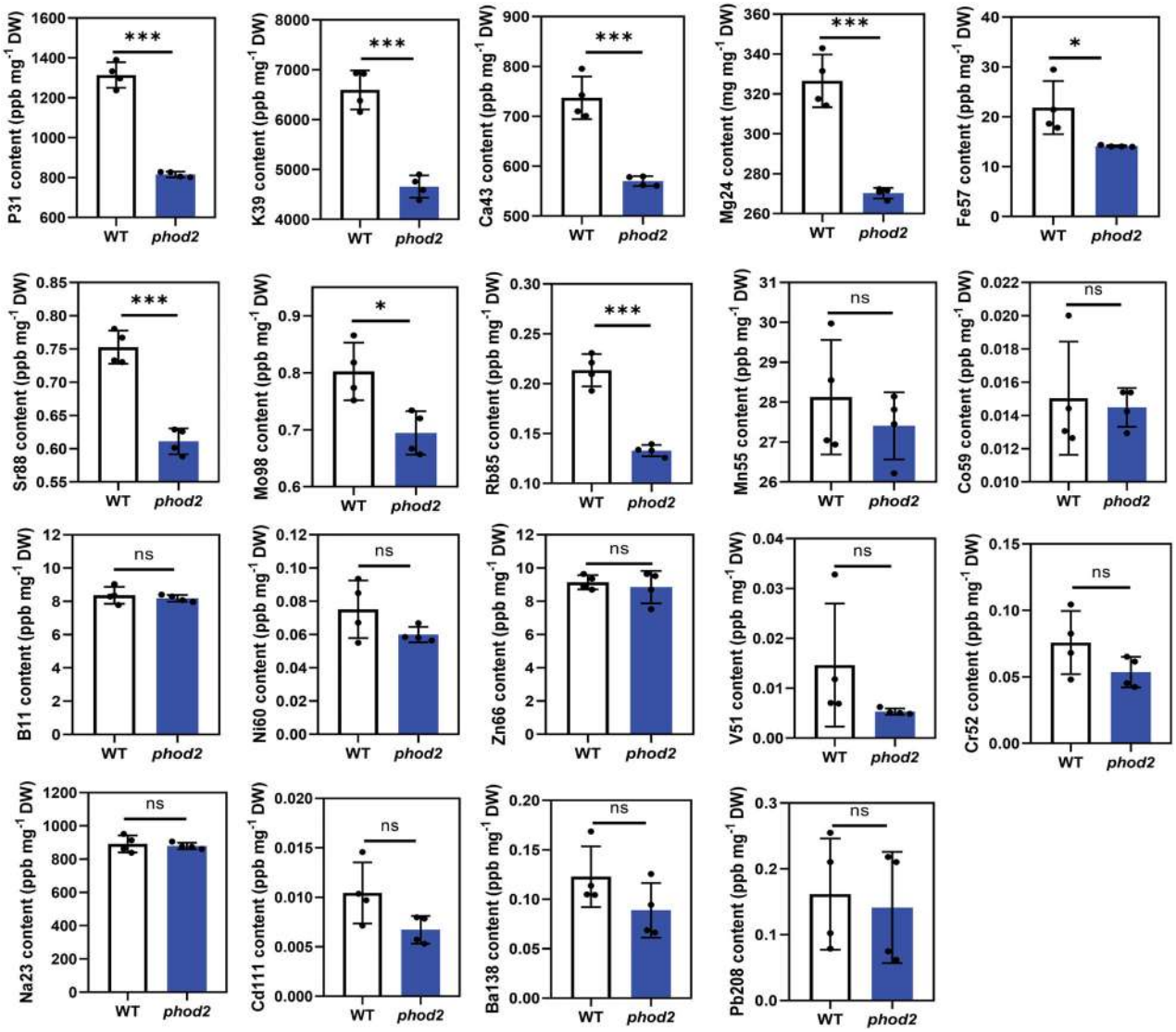


**Figure 8.** Absence of LIP1p perturbed ion homeostasis in *phod2* mutant. Ionomics analysis in 14-day-old seedlings of WT and *phod2* mutant grown on an HP medium. DW, dry weight. The data are means ± SD. $n = 4$. *$P < 0.05$, ***$P < 0.001$, two-tailed *t*-test.

produce acetyl-coenzyme A (acetyl-CoA) for the de novo fatty acid synthesis.

There are plastid-specific octanoyltransferase LIP2p and lipoyl synthase LIP1p to catalyze the lipoylation of PHD (Wada, Yasuno, & Wada, 2001; Yasuno & Wada, 2002). Mutation of *LIP1p* or the two isoforms of *LIP2p* (*LIP2p1* and *LIP2p2*) resulted in embryo-lethality (Ewald, Hoffmann, Neuhaus, & Bauwe, 2014). However, *phod2* is able to complete its life cycle, and a genomic construct of *LIP1p* successfully rescued the mutant phenotype, demonstrating that *phod2* is a weak allele of *LIP1p* (Figure S2). Genomic sequence analysis revealed a point mutation at the last nucleotide of the fifth exon. RT-PCR analysis indicated an intron was retained in most *LIP1p* transcripts, which was further confirmed by the Sanger sequencing (Figure 4b–d).

The embryonic lethality of *LIP1p* null allele makes it difficult to analyze its function in vivo (Ewald et al., 2014). So, *phod2* allele is an ideal genetic material to study *LIP1p* function. LIP1p is specifically localized in plastids and required for the function of pyruvate dehydrogenase (PDH) involved in fatty acid biosynthesis. So, the LIP1p may play a direct role in regulating lipid homeostasis. Lipidomic analyses revealed that lipid homeostasis was disrupted in *phod2* mutant. Interestingly, the contents of many species of PA, PC, PE, and PG were significantly decreased in *phod2* (Figure 7). More and more evidences suggest that lipid homeostasis is critical for vesicle trafficking in secretory pathways (Melser et al., 2011). For example, phospholipase D (PLD) and phosphatidic acid (PA) regulated vesicle trafficking and auxin transport in *Arabidopsis* (Li & Xue, 2007);

C26-sphingolipids were involved in the transport of the Pma1 ATPase to the plasma membrane in yeast (Gaigg, Timischl, Corbino, & Schneiter, 2005); Mutation of choline transporter CTL1 perturbed vesicle trafficking of ion transporters and ion homeostasis through the effects on PLD, phosphatidylcholines (PC) and phosphatidylethanolamines (PE) (Gao et al., 2017). In this study, we found the abundance of phosphate transporters at the plasma membrane was decreased in *phod2* (Figure 6). PHT1s are regulated at both transcriptional and posttranslational levels. In *phod2* mutants, the transcript levels of *PHT1;4* were increased (Figure 1b) and a higher PHT1-GFP signal was detected in the cytosol (Figure 6b). The trafficking of PHT1 proteins is also tightly regulated to maintain Pi homeostasis. ALIX associates with ESCRI–III complex and participates in the trafficking of PHT1 from the PM to the vacuole (Cardona-López et al., 2015). Upon BFA treatment, the PHT1;4-GFP in *trans*-Golgi network and early endosome accumulated in BFA compartments (Bayle et al., 2011; Figure 6e). However, the accumulated GFP signal was greatly reduced in *phod2* mutant, indicating that PHT1 proteins were sequestered in the ER or *cis*-Golgi (Figure 6e). The *phod2* mutation disrupted lipid homeostasis which is critical for Golgi membrane dynamics and vesicular transport of proteins (Figure 7; Melser et al., 2011). Thus, LIP1p regulates the trafficking of PHT1 at a stage earlier than regulated by ALIX, but later than PHF1 (Bayle et al., 2011; Cardona-López et al., 2015; González et al., 2005). The compromised function of transporters greatly reduced Pi uptake and the content of Pi in *phod2* mutant was much lower than that in WT and the overexpression of *PHT1;1* could partially rescue Pi deficiency in *phod2* (Figures S2g, S4). However, the root length was not changed by *PHT1;1* expression (Figure S4), as the root phenotype is a local regulatory response (Svistoonoff et al., 2007; Thibaud et al., 2010). The enhanced expression of PSI genes and PSR phenotypes in *phod2* mutant are the direct effect of Pi deficiency (Figure 5). These results suggest that LIP1p may regulate the trafficking of PHT1 to PM to maintain Pi homeostasis.

However, *LIP1p* is not specifically induced by low phosphate (Figures S7). We also realized that the effects of *LIP1p* mutation on Pi transporters are not specific, as different elements were differentially affected. *LIP1p* mutation significantly disrupted the homeostasis of a series of mineral nutrients, including K, Ca, Mg, Fe, Sr, Mo, and Rb, suggesting that LIP1p has a systemic impact on vesicle trafficking of different ion transporters (Figure 8). The genes involved in sulpholipids or galactolipids biogenesis were significantly induced in *phod2* (Figure S7). The phospholipid-to-sulpholipid and phospholipid-to-galactolipid membrane lipid remodeling could improve the internal phosphorus utilization efficiency (PUE) under low phosphate conditions (Heuer et al., 2017).

In summary, this study employed a reporter-based forward genetic approach to identify the plastidial lipoyl synthase LIP1p as a novel regulator of Pi homeostasis. The upregulation of PSI genes and the PSR phenotypes observed in *phod2*-mutant result from Pi deficiency, as the disruption of lipid homeostasis likely impairs perturb PHT1 trafficking to the plasma membrane. Furthermore, LIP1p-mediated lipid homeostasis impacts multiple ion homeostasis, implying it broadly supports vesicle trafficking for various ion transporters. Our findings offer strong genetic evidence that lipid homeostasis is essential for nutrient homeostasis by maintaining vesicle trafficking of ion transporters in plants.

## MATERIALS AND METHODS

### Plant materials and growth conditions

The transgenic line *pPHT1;4::LUC* described previously as the WT in this study (Lei *et al.*, 2011). The *35S::PHT1;1-GFP/phod2* was generated by a genetic cross between *35S::PHT1;1-GFP* and *phod2*. The *pPHT1;1::PHT1;1-GFP/phod2* and *pPHT1;4::PHT1;4-GFP/phod2* were generated by a genetic cross between *pPHT1;1::PHT1;1-GFP* or *pPHT1;4::PHT1;4-GFP* with *phod2*. The seeds were surface sterilized in 20% bleach for 10 min and washed four times with sterile deionized water, kept at 4°C for 2 days. The sterilized seeds were grown on a medium containing 1/2 MS nutrients in the growth chamber at 23°C under a photoperiod of 16 h light/8 h dark. HP (high phosphate) and LP (low phosphate) agar media contain 625 μM and 150 μM Pi, respectively, with other basic 1/2 MS nutrients.

### Plasmid construction and complementation analysis

For complementation, *LIP1p* genomic DNA with about 2 kb of promoter region was amplified from Col-0 genomic DNA and cloned into pCAMBIA1300 vector harboring a FLAG tag by the homologous recombination method. The construct was transformed into *phod2* plants.

### Quantification of Pi content

Tissues from whole 8-day-old seedlings were collected, and the fresh weight was recorded. The tissues were then snap-frozen in liquid nitrogen and ground into a fine powder. Pi content was then measured using the phosphomolybdate colorimetric assay (Jain et al., 2007).

### Real-time quantitative PCR

Total RNA was extracted from seedlings using the RNeasy Plant Mini Kit (Qiagen, R415102), and 1 μg of total RNA was reverse-transcribed following the instructions (Yeasen, 11137ES60). Real-time PCR was performed using a CFX96 real-time PCR detection system (Bio-Rad, USA) using a qPCR SYBR Green Master Mix (Yeasen, 11201ES08). *ACTIN2* was used as an internal control gene.

### RNA-seq analysis

Total RNAs were extracted from 8-day-old seedlings under HP or LP conditions using an RNeasy Plant Mini Kit (Qiagen, R415102) according to the instruction manual. Three biological replicates were performed for each genotype. The genes that were

upregulated or downregulated with a twofold or higher change with an adjusted *P* value of ≤0.05 were regarded as DEGs. Venn diagrams were created using Venny (2.1.0). GO enrichment analysis was performed using clusterProfiler (v.4.0.5) (Yu, Wang, Han, & He, 2012).

### Western blotting

To determine the protein levels of PHT1;1-GFP and PHT1;4-GFP, 8-day-old seedling tissues were ground into fine powder in liquid nitrogen and 5% SDS was added. The solution was then boiled at 98°C for 10 min and centrifuged at 13000 rpm for 10 min. The supernatant was mixed with 5× SDS loading buffer and separated by 10% SDS–PAGE gel. The types of protein antibodies we use are as follows: anti-GFP (Roch, 11 814 460 001, 1:10000 dilution), anti-ACTIN (CWBIO, CW0265, 1:5000 dilution), anti-Rabbit&Mouse (IgG-HRP, M21003L, 1:8000).

### Anthocyanin content measurement

Tissues were collected from 12-day-old seedlings, quick-frozen in liquid nitrogen, and ground into powder. Anthocyanin was extracted with methanol containing 1% HCl (v/v). The anthocyanin content was measured as previously described (Bieza & Lois, 2001). The anthocyanin contents were calculated as $A_{530\text{-}657}$ $g^{-1}$ fresh weight.

### Elemental analysis

*Arabidopsis thaliana* tissue elemental analysis via ICP-MS has been previously described (Chao et al., 2014). The samples were transferred to an oven for 20 h at 92°C and then weighed with an analytical balance. Four biological replicates were performed for each genotype. All samples were digested with 1 mL of concentrated nitric acid containing indium (In) for 4 h at 110°C. Finally, the samples are diluted to 10 mL with 18 MΩ of water. Elemental analysis of B, Na, Mg, Al, P, Ca, V, Cr, Mn, Fe, Co, Ni, Cu, Zn, As, Se, Rb, Sr, Mo, Cd, Ba, Pt, Pb, and K were performed with ICP-MS (NexION 350D; PerkinElmer, Waltham, MA) coupled with an Apex desolvation system and an SC-4 DX autosampler (Elemental Scientific Inc., Omaha, NE).

### Lipid extraction and determination

Ten-day-old Arabidopsis seedlings growing on Petri plates were used for lipid extraction. Six replicates of approximately 100 mg were performed. Plant lipidomic analysis via LC–MS has been previously described (Narváez-Rivas & Zhang, 2016). Chromatographic separation was accomplished in a Thermo Ultimate 3000 system equipped with an ACQUITY UPLC® BEH C18 (100 × 2.1 mm, 1.7 μm, Waters) column maintained at 50°C. The ESI-MSn experiments were executed on the Thermo Q Exactive Focus mass spectrometer with the spray voltage of 3.5 kV and −2.5 kV in positive and negative modes, respectively. For this experiment, agglomerate hierarchical clustering was used, each object is grouped into a class and the classes are merged to become larger and larger objects until the end. The data set was scaled by the pheatmap package in R (v3.3.2) to obtain a hierarchical clustering map of relative quantitative values of lipids.

## ACCESSION NUMBERS

All high-throughput sequencing data generated in this study were submitted to NCBI's Gene Expression Omnibus (GSE278345). Additional data set used in this study are GSE16722 (Bustos et al., 2010).

## AUTHOR CONTRIBUTIONS

*Conceptualization*: SG, XX, and ML; *Methodology*: SG and XX; *Investigation*: SG, XX, KZ, CY, JD, KC, and QL; *Writing—review and editing*: SG, XX, VS, and ML; *Supervision*: ML.

## ACKNOWLEDGMENTS

This work was sponsored by Hangzhou Normal University (KYQD-2024-305) and the Youth Innovation Promotion Association CAS (No. 2023285).

## CONFLICT OF INTEREST

The authors declare no competing interests.

## DATA AVAILABILITY STATEMENT

All relevant data can be found within the manuscript and its supporting materials.

## SUPPORTING INFORMATION

Additional Supporting Information may be found in the online version of this article.

**Figures S1.** The genetic screens using a reporter gene for elucidating phosphate transport or phosphate starvation response mechanism. (a) Luciferase gene (LUC) acts as the reporter gene that driven by a promoter of *PHT1;4*. (b) The reporter gene was specifically induced by phosphate starvation which presented by luminescence signals. HP (High phosphate, 625 μM), LP (Low phosphate, 150 μM). Scale bars, 0.5 cm. (c) Schematic diagram of the process for mutants screening involved in phosphate transport or phosphate starvation.

**Figure S2.** Growth and developmental phenotypes of *phod2* mutant. (a) The primary root length of WT and *phod2* mutant grown on HP or LP conditions. The data are means ± SD. $n = 15$. $^{*}P < 0.05$, $^{**}P < 0.01$, $^{***}P < 0.001$. Two-tailed *t*-test. (b) Leaf size of WT and the *phod2* mutant. Scale bars, 0.5 cm. 3 weeks seedlings. (c) Seeds development of WT and the *phod2* mutant. Red arrows indicate the aborted ovules. Arranged from top to bottom in a morphological apical to basal. Scale bars, 1 mm. (d) Plant height of WT and the *phod2* mutant at 6 weeks. (e) The plant dry biomass of 10-day-old seedlings on HP or LP media, each sample contains 60 plants. The data are means ± SD. $n = 6$ (biological replicates). (f) Pi content in the shoots and roots of the WT and *phod2* mutant on HP or LP media. The data are means ± SD. $n = 3/5$ (biologically independent replicates). (g) Root hair phenotypes of 10-day-old WT and *phod2* seedlings on HP or LP media. Scale bar, 1mm.

**Figure S3.** RNA structure prediction shows $LIP1^{pG996A}$ leading to changes in pre-mRNA splicing. (a) RNA structure was predicted by the region of the fifth exon-intron-exon of the *LIP1p* gene. The red arrow represents the position of single-base substitution in *LIP1p*. (b) RNA-predicted structure of wildtype *LIP1p*. (c) RNA-predicted structure of *LIP1p* when single-base substitution (G996A). RNA structure prediction was performed by RNAfold in the Vienna package (Ver.2.4.3). Red represents the high probability of base pairing.

**Figure S4.** Overexpression of *PHT1;1* partly restored Pi content of *phod2*. (a) Quantitative real-time. PCR analysis of *PHT1;1* transcript levels in WT, *phod2*, *1#35S::PHT1;1-GFP/phod2* and *2#35S::PHT1;1-GFP/phod2* on HP condition. The data are means ± SD. $n = 3$ (biological replicates). (b) Overexpression of *PHT1;1* in

*phod2* can significantly elevate Pi content in the mutant. The data are means ± SD. $n = 4/6$ (biological replicates). $*P < 0.05$, $**P < 0.01$, $***P < 0.001$, two-tailed *t*-test. (c) The root phenotype among WT, *phod2, 1#35S::PHT1;1-GFP/phod2* and *2#35S::PHT1;1-GFP/phod2* on HP condition. Scale bars, 1 cm. (d) Overexpressed of PHT1;1 by *35S* promoter in root epidermal cells of *phod2*. 8-day-old seedlings grown on LP (150 μM Pi) condition. Native promoter driven *PHT1;1-GFP* acts as the control.

**Figure S5.** Volcano plots show the differentially expressed metabolites in each lipid class.

**Figure S6.** Overexpression of *PHT1;1* in *phod2* partly restored the lipid metabolites level. (a) Agglomerate hierarchical clustering heatmap indicates the DE metabolites between *PHT1;1OE/phod2* and *phod2*. (b) Number of DE lipid metabolites in *PHT1;1-OE/phod2* compared with *phod2*. (c) Overlap of metabolites that Down-regulated in *phod2* while up-regulated in *PHT1;1OE/phod2*. (d) Overlap of metabolites that up-regulated in *phod2* while down-regulated in *PHT1;1OE/phod2*. the number in parenthesis represent the metabolites number. (e) Heatmap shows the content of 60 lipid metabolites decrease in *phod2* while significantly elevated by overexpression of *PHT1;1*. (f) Heatmap shows the content of 18 lipid metabolites increase in *phod2* while significantly reduce by overexpression of *PHT1;1*.

**Figure S7.** Relative gene expressions of MGDs, DGDs and LIP1p genes in 8-day-old WT and *phod2* seedlings on HP or LP media. The data are means ± SD. $n = 3$ (biologically replicates).

**Figure S8.** Ion transporters are induced in *phod2* mutant. Heatmap cluster of transcripts of ion transporter genes which was upregulated in the *phod2* mutant grown under HP condition.

**Data S2.** Supporting Information.

**Data S3.** Supporting Information.

## REFERENCES


**Bayle, V., Arrighi, J.F., Creff, A., Nespoulous, C., Vialaret, J., Rossignol, M. *et al.*** (2011) Arabidopsis thaliana High-Affinity Phosphate Transporters Exhibit Multiple Levels of Posttranslational Regulation. *Plant Cell*, **23**, 1523–1535.

**Bieleski, R.L.** (1973) Phosphate Pools, Phosphate Transport, and Phosphate Availability. *Annual Review of Plant Physiology*, **24**, 225–252.

**Bieza, K.** & **Lois, R.** (2001) An Arabidopsis Mutant Tolerant to Lethal Ultraviolet-B Levels Shows Constitutively Elevated Accumulation of Flavonoids and Other Phenolics. *Plant Physiology*, **126**, 1105–1115.

**Burger, J.** & **Edwards, G.E.** (1996) Photosynthetic efficiency, and photodamage by UV and visible radiation, in red versus green leaf Coleus varieties. *Plant & Cell Physiology*, **37**, 395–399.

**Bustos, R., Castrillo, G., Linhares, F., Puga, M.I., Rubio, V., Pérez-Pérez, J. *et al.*** (2010) A Central Regulatory System Largely Controls Transcriptional Activation and Repression Responses to Phosphate Starvation in Arabidopsis. *PLoS Genetics*, **6**, e1001102.

**Cardona-López, X., Cuyas, L., Marín, E., Rajulu, C., Irigoyen, M.L., Gil, E. *et al.*** (2015) ESCRT-III-Associated Protein ALIX mediates high-affinity phosphate transporter trafficking to maintain phosphate homeostasis in Arabidopsis. *Plant Cell*, **27**, 2560–2581.

**Chao, D.Y., Chen, Y., Chen, J.G., Shi, S.L., Chen, Z.R., Wang, C.C. *et al.*** (2014) Genome-wide Association mapping identifies a new arsenate reductase enzyme critical for limiting arsenic accumulation in plants. *PLoS Biology*, **12**, e1002009.

**Chen, J.Y., Wang, Y.F., Wang, F., Yang, J., Gao, M.X., Li, C.Y. *et al.*** (2015) The rice CK2 kinase regulates trafficking of phosphate transporters in response to phosphate levels. *Plant Cell*, **27**, 711–723.

**Douce, R., Bourguignon, J., Neuburger, M.** & **Rebeille, F.** (2001) The glycine decarboxylase system: A fascinating complex. *Trends in Plant Science*, **6**, 167–176.

**Ewald, R., Hoffmann, C., Neuhaus, E.** & **Bauwe, H.** (2014) Two redundant octanoyltransferases and one obligatory lipoyl synthase provide protein-lipoylation autonomy to plastids of Arabidopsis. *Plant Biology*, **16**, 35–42.

**Gaigg, B., Timischl, B., Corbino, L.** & **Schneiter, R.** (2005) Synthesis of Sphingolipids with very long chain fatty acids but not Ergosterol is required for routing of newly synthesized plasma membrane ATPase to the cell surface of yeast. *The Journal of Biological Chemistry*, **280**, 22515–22522.

**Gao, Y.Q., Chen, J.G., Chen, Z.R., An, D., Lv, Q.Y., Han, M.L. *et al.*** (2017) A new vesicle trafficking regulator CTL1 plays a crucial role in ion homeostasis. *PLoS Biology*, **15**, e2002978.

**González, E., Solano, R., Rubio, V., Leyva, A.** & **Paz-Ares, J.** (2005) PHOSPHATE TRANSPORTER TRAFFIC FACILITATOR1 is a plant-specific SEC12-related protein that enables the endoplasmic reticulum exit of a high-affinity phosphate transporter in Arabidopsis. *Plant Cell*, **17**, 3500–3512.

**Gosai, S.J., Foley, S.W., Wang, D.X., Silverman, I.M., Selamoglu, N., Nelson, A.D.L. *et al.*** (2015) Global Analysis of the RNA-Protein Interaction and RNA Secondary Structure Landscapes of the Arabidopsis Nucleus. *Molecular Cell*, **57**, 376–388.

**Heuer, S., Gaxiola, R., Schilling, R., Herrera-Estrella, L., López-Arredondo, D., Wissuwa, M. *et al.*** (2017) Improving phosphorus use efficiency: a complex trait with emerging opportunities. *The Plant Journal*, **90**, 868–885.

**Jain, A., Poling, M.D., Karthikeyan, A.S., Blakeslee, J.J., Peer, W.A., Titapiwatanakun, B. *et al.*** (2007) Differential effects of sucrose and auxin on localized phosphate deficiency-induced modulation of different traits of root system architecture in Arabidopsis. *Plant Physiology*, **144**, 232–247.

**Karthikeyan, A.S., Varadarajan, D.K., Mukatira, U.T., D'Urzo, M.P., Damsz, B.** & **Raghothama, K.G.** (2002) Regulated expression of Arabidopsis Phosphate transporters. *Plant Physiology*, **130**, 221–233. https://doi.org/10.1104/pp.020007

**Lei, M.G., Liu, Y.D., Zhang, B.C., Zhao, Y.T., Wang, X.J., Zhou, Y.H. *et al.*** (2011) Genetic and Genomic Evidence That Sucrose Is a Global Regulator of Plant Responses to Phosphate Starvation in Arabidopsis. *Plant Physiology*, **156**, 1116–1130.

**Lei, M.G., Zhu, C.M., Liu, Y.D., Karthikeyan, A.S., Bressan, R.A., Raghothama, K.G. *et al.*** (2011) Ethylene signalling is involved in regulation of phosphate starvation-induced gene expression and production of acid phosphatases and anthocyanin in. *The New Phytologist*, **189**, 1084–1095.

**Li, G.** & **Xue, H.W.** (2007) Arabidopsis PLDzeta2 regulates vesicle trafficking and is required for auxin response. *Plant Cell*, **19**, 281–295.

**Liu, Z.S., Liu, Q., Yang, X.F., Zhang, Y.Y., Norris, M., Chen, X.X. *et al.*** (2021) In vivo nuclear RNA structurome reveals RNA-structure regulation of mRNA processing in plants. *Genome Biology*, **22**, 11.

**Lopez-Bucio, J., Cruz-Ramirez, A.** & **Herrera-Estrella, L.** (2003) The role of nutrient availability in regulating root architecture. *Current Opinion in Plant Biology*, **6**, 280–287.

**Lorenz, R., Bernhart, S.H., Siederdissen, C.H.Z., Tafer, H., Flamm, C., Stadler, P.F. *et al.*** (2011) ViennaRNA Package 2.0. *Algorithm. Molecular Biology*, **6**, 26.

**Melser, S., Molino, D., Batailler, B., Peypelut, M., Laloi, M., Wattelet-Boyer, V. *et al.*** (2011) Links between lipid homeostasis, organelle morphodynamics and protein trafficking in eukaryotic and plant secretory pathways. *Plant Cell Reports*, **30**, 177–193.

**Misson, J., Thibaud, M.C., Bechtold, N., Raghothama, K.** & **Nussaume, L.** (2004) Transcriptional regulation and functional properties of Arabidopsis Pht1;4, a high affinity transporter contributing greatly to phosphate uptake in phosphate deprived plants. *Plant Molecular Biology*, **55**, 727–741.

**Mooney, B.P., Miernyk, J.A.** & **Randall, D.D.** (2002) The complex fate of alpha-ketoacids. *Annual Review of Plant Biology*, **53**, 357–375.

**Narváez-Rivas, M.** & **Zhang, Q.B.** (2016) Comprehensive untargeted lipidomic analysis using core-shell C30 particle column and high field orbitrap mass spectrometer. *Journal of Chromatography. A*, **1440**, 123–134.

**Peret, B., Desnos, T., Jost, R., Kanno, S., Berkowitz, O.** & **Nussaume, L.** (2014) Root Architecture Responses: In Search of Phosphate. *Plant Physiology*, **166**, 1713–1723.

**Perham, R.N.** (2000) Swinging arms and swinging domains in multifunctional enzymes: Catalytic machines for multistep reactions. *Annual Review of Biochemistry*, **69**, 961–1004.

**Shin, H., Shin, H.S., Dewbre, G.R.** & **Harrison, M.J.** (2004) Phosphate transport in Arabidopsis: Pht1;1 and Pht1;4 play a major role in phosphate acquisition from both low- and high-phosphate environments. *The Plant Journal*, **39**, 629–642.

**Svistoonoff, S., Creff, A., Reymond, M., Sigoillot-Claude, C., Ricaud, L., Blanchet, A. *et al.*** (2007) Root tip contact with low-phosphate media reprograms plant root architecture. *Nature Genetics*, **39**, 792–796.

**Thibaud, M.C.**, **Arrighi, J.F.**, **Bayle, V.**, **Chiarenza, S.**, **Creff, A.**, **Bustos, R.** ***et al.*** (2010) Dissection of local and systemic transcriptional responses to phosphate starvation in Arabidopsis. *The Plant Journal*, **64**, 775–789.

**Tran, H.T.**, **Hurley, B.A.** & **Plaxton, W.C.** (2010) Feeding hungry plants: The role of purple acid phosphatases in phosphate nutrition. *Plant Science*, **179**, 14–27.

**Vance, C.P.**, **Uhde-Stone, C.** & **Allan, D.L.** (2003) Phosphorus acquisition and use: critical adaptations by plants for securing a nonrenewable resource. *The New Phytologist*, **157**, 423–447.

**Wada, M.**, **Yasuno, R.**, **Jordan, S.W.**, **Cronan, J.E.** & **Wada, H.** (2001) Lipoic acid metabolism in Arabidopsis thaliana Cloning and characterization of a cDNA encoding lipoyltransferase. *Plant & Cell Physiology*, **42**, 650–656.

**Wada, M.**, **Yasuno, R.** & **Wada, M.** (2001) Identification of an Arabidopsis cDNA encoding a lipoyltransferase located in plastids. *FEBS Letters*, **506**, 286–290.

**Wang, L.S.**, **Li, Z.**, **Qian, W.Q.**, **Guo, W.L.**, **Gao, X.**, **Huang, L.L.** ***et al.*** (2011) The Arabidopsis Purple Acid Phosphatase AtPAP10 Is Predominantly Associated with the Root Surface and Plays an Important Role in Plant Tolerance to Phosphate Limitation. *Plant Physiology*, **157**, 1283–1299.

**Xiao, X.L.**, **Zhang, J.Q.**, **Satheesh, V.**, **Meng, F.X.**, **Gao, W.L.**, **Dong, J.S.** ***et al.*** (2022) SHORT-ROOT stabilizes PHOSPHATE1 to regulate phosphate allocation in. *Nature Plants*, **8**, 1074–1081.

**Yang, Z.L.**, **Yang, J.**, **Wang, Y.**, **Wang, F.**, **Mao, W.X.**, **He, Q.J.** ***et al.*** (2020) PROTEIN PHOSPHATASE95 Regulates Phosphate Homeostasis by Affecting Phosphate Transporter Trafficking in Rice. *Plant Cell*, **32**, 740–757.

**Yasuno, R.** & **Wada, H.** (1998) Biosynthesis of lipoic acid in Arabidopsis: Cloning and characterization of the cDNA for lipoic acid synthase. *Plant Physiology*, **118**, 935–943.

**Yasuno, R.** & **Wada, H.** (2002) The biosynthetic pathway for lipoic acid is present in plastids and mitochondria in Arabidopsis thaliana. *FEBS Letters*, **517**, 110–114.

**Yu, G.C.**, **Wang, L.G.**, **Han, Y.Y.** & **He, Q.Y.** (2012) clusterProfiler: an R Package for Comparing Biological Themes Among Gene Clusters. *OMICS*, **16**, 284–287.